

Polarization of skylight in the O₂A band: effects of aerosol properties

Eyk Boesche,^{1,*} Piet Stammes,^{2,4} Réne Preusker,¹ Ralf Bennartz,^{3,5}
Wouter Knap,² and Juergen Fischer¹

¹Free University Berlin, Institute for Space Sciences, Carl-Heinrich-Becker-Weg 6-10, 12165 Berlin, Germany

²Royal Netherlands Meteorological Institute (KNMI), PO Box 201, 3730 AE De Bilt, the Netherlands

³Department of Atmospheric and Oceanic Sciences, University of Wisconsin,
1225 W. Dayton St., Madison, Wisconsin 53706, USA

⁴E-mail: stammes@knmi.nl

⁵E-mail: bennartz@aos.wisc.edu

*Corresponding author: boesche@knmi.nl

Received 4 February 2008; accepted 8 May 2008;
posted 22 May 2008 (Doc. ID 92253); published 24 June 2008

Motivated by several observations of the degree of linear polarization of skylight in the oxygen A (O₂A) band that do not yet have a quantitative explanation, we analyze the influence of aerosol altitude, microphysics, and optical thickness on the degree of linear polarization of the zenith skylight in the spectral region of the O₂A band, between 755 to 775 nm. It is shown that the degree of linear polarization inside the O₂A band is particularly sensitive to aerosol altitude. The sensitivity is strongest for aerosols within the troposphere and depends also on their microphysical properties and optical thickness. The polarization of the O₂A band can be larger than the polarization of the continuum, which typically occurs for strongly polarizing aerosols in an elevated layer, or smaller, which typically occurs for depolarizing aerosols or cirrus clouds in an elevated layer. We show that in the case of a single aerosol layer in the atmosphere a determination of the aerosol layer altitude may be obtained. Furthermore, we show limitations of the aerosol layer altitude determination in case of multiple aerosol layers. To perform these simulations we developed a fast method for multiple scattering radiative transfer calculations in gaseous absorption bands including polarization. The method is a combination of doubling-adding and k-binning methods. We present an error estimation of this method by comparing with accurate line-by-line radiative transfer simulations. For the O₂A band, the errors in the degree of linear polarization are less than 0.11% for transmitted light, and less than 0.31% for reflected light. © 2008 Optical Society of America

OCIS codes: 010.1110, 260.5430, 280.1310, 101.320, 300.1030.

1. Introduction

Polarization observations of reflected or transmitted skylight in absorption bands, such as the oxygen A (O₂A) band or water vapor bands, show prominent features due to molecular absorption. For ground-based polarization measurements of transmitted skylight in the spectral region of the O₂A band these

features are apparent in observations taken by Stammes *et al.* [1], Preusker *et al.* [2], and Aben *et al.* [3,4]. These authors have shown that on cloudless days the degree of linear polarization within the O₂A absorption band, around 760 nm, can be significantly higher or lower than the absorption-free continuum polarization (see Fig. 1). According to Stammes *et al.*, the strong molecular absorption within the absorption band can explain the difference in polarization between continuum and absorption band. The strong absorption is shielding lower layers of the

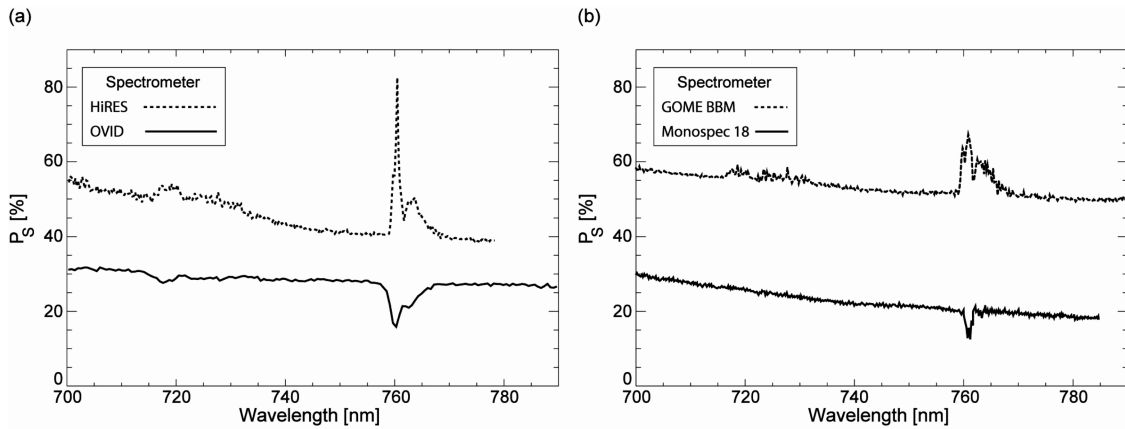


Fig. 1. Ground-based measurements of the degree of linear polarization P_s of the cloud free sky as a function of wavelength. (a) As measured at the Institute for Space Sciences, in Berlin, Germany (52.5° N, 13.3° E) on 11 May 1994 with the spectrometer OVID (solid line) with a spectral resolution of 2.0 nm, and as measured on 24 June 1994 with the spectrometer HiRES (dotted line) with a spectral resolution of 0.3 nm [2]. Geometry on both days: solar zenith angle $\theta_0 \approx 40^\circ$, viewing zenith angle $\theta = 60^\circ$, azimuth angle $\phi - \phi_0 = 180^\circ$, and scattering angle $\Theta = 100^\circ$. (b) As measured at SRON, Utrecht, the Netherlands (52.1° N, 5.2° E) on 7 April 1997 with the spectrometer GOME BBM with a spectral resolution of 0.33 nm at a solar zenith angle of $\theta_0 = 79^\circ$, viewing zenith angle of $\theta = 0^\circ$, and scattering angle of $\Theta = 79^\circ$ (dotted line) [3], and as measured on 19 October 1993 at KNMI, in De Bilt, the Netherlands (52.1° N, 5.2° E) with a Jarrell Ash Monospec 18 spectrometer with a spectral resolution of 0.3 nm at a solar zenith angle of $\theta_0 = 66^\circ$, viewing zenith angle of $\theta = 0^\circ$, and scattering angle of $\Theta = 66^\circ$ (solid line) [1].

atmosphere from incident sunlight. Therefore most of the light has been scattered at high altitudes, whereas in the continuum no such shielding occurs. Thus, if the polarization properties of the lower atmospheric layers differ from those of the upper layers, a change of polarization can occur between the polarization in the continuum and the absorption band. Aerosol layers could especially cause such a change. Ground-based measurements of the polarization of the clear zenith sky in the O₂A band may offer information on the aerosol altitude profile [1,2,5].

In this paper we analyze the sensitivity of the degree of linear polarization of transmitted skylight in the spectral region of the O₂A band, between 755 and 775 nm, to changes of aerosol altitude, aerosol microphysics, and aerosol optical thickness (in the troposphere and lower stratosphere), extending the above mentioned work. To adequately study the effect of aerosol altitude on polarization of skylight in the O₂A band, we combined two existing radiative transfer methods to significantly improve the calculation time while maintaining a high accuracy compared to line-by-line simulations. As a spectral approximation technique we use the k-binning method, which is similar to a k-distribution approach, but overcomes shortcomings of a conventional k-distribution [6,7]. We integrate this method in monochromatic doubling-adding multiple scattering calculations, including polarization, for vertically inhomogeneous atmospheres. An advantage of our combined method approach is that an implementation of a different response function is straightforward and does not require a new set of multiple scattering simulations. For our study we use spectral response functions with a resolution of 0.36 nm at full width at half-maximum (FWHM) and an equal spacing of 0.21 nm. As atmospheric scatterers, we use Rayleigh scattering mole-

cules and spherical aerosols as well as nonspherical ice crystal particles, using Mie-theory and the geometric-optics (GO) approximation.

In Section 2 the definition of relevant polarization parameters, such as Stokes parameters, and the scattering matrix, are briefly discussed. Furthermore, we describe our combined method for fast radiative transfer simulations in absorption bands including polarization and give an error estimation of this method by comparing with accurate line-by-line radiative transfer simulations. In Section 3 we show the sensitivity of the degree of linear polarization of the zenith skylight to aerosol altitude and aerosol optical thickness within the O₂A absorption band and for the absorption-free continuum. Furthermore, we show the influence of the solar zenith angle, and spectral response function on the degree of linear polarization of the zenith skylight. The summary and conclusions follow in Section 4.

2. Combined Method for Fast Simulations of the Degree of Polarization in Absorption Bands

A. Stokes Parameters and Polarization

The state of polarization of a light beam can be defined through the components of the Stokes vector \mathbf{I} [8,9], by measuring the relative intensities I_α of the light beam after it has passed through polarization devices at different orientation angles α of their transmission axes [10]:

$$\mathbf{I} = \begin{pmatrix} I \\ Q \\ U \\ V \end{pmatrix} = \begin{pmatrix} I_{0^\circ} + I_{90^\circ} \\ I_{0^\circ} - I_{90^\circ} \\ I_{45^\circ} - I_{135^\circ} \\ I_+ - I_- \end{pmatrix}, \quad (1)$$

where 0°, 45°, 90°, and 135° denote the orientation

angle of the polarization transmission axis with respect to a reference plane, and + and – are the right- and left-handed circular polarization components. The Stokes parameter I describes the total intensity, Q and U the linear polarization and V the circular polarization of the light beam. The degree of linear polarization in terms of Stokes parameters is defined as follows [11]:

$$P = \frac{(Q^2 + U^2)^{1/2}}{I}. \quad (2)$$

In case $U = 0$, the following alternative definition for the degree of linear polarization will be used:

$$P_s = -\frac{Q}{I}. \quad (3)$$

For $P_s < 0$ and $P_s > 0$, the light is polarized parallel and perpendicular to the reference plane, respectively.

B. Scattering Matrix at 765 nm

The scattering matrix F describes the change of direction, intensity, and polarization of a light beam caused by a single scattering event. The Stokes parameters of the scattered beam at scattering angle Θ can be written as a linear transformation of the Stokes parameters of the incident beam. We consider independent light scattering by an ensemble of randomly oriented particles, which have a plane of symmetry. Then the scattering matrix of the ensemble takes the following form [8,10,11]:

$$\begin{pmatrix} I_{\text{sca}} \\ Q_{\text{sca}} \\ U_{\text{sca}} \\ V_{\text{sca}} \end{pmatrix} = \begin{bmatrix} F_{11} & F_{12} & 0 & 0 \\ F_{12} & F_{22} & 0 & 0 \\ 0 & 0 & F_{33} & F_{34} \\ 0 & 0 & -F_{34} & F_{44} \end{bmatrix} \begin{pmatrix} I_{\text{in}} \\ Q_{\text{in}} \\ U_{\text{in}} \\ V_{\text{in}} \end{pmatrix}, \quad (4)$$

where the subscripts “sca” and “in” stand for scattered and incoming beams. The scattering matrix elements F_{ij} are functions of the scattering angle. The function F_{11} is called the phase function and is normalized to 1. For unpolarized incident light only the first column of the scattering matrix suffices to determine the intensity and the state of polarization of the light scattered once. In this case F_{11} is proportional to the scattered intensity as a function of the scattering angle and, furthermore, the degree of linear polarization is represented by the ratio $-F_{12}/F_{11}$. F depends on the wavelength, the refractive index, the size distribution, and the shape of the scattering particles and contains all polarizing properties of the ensemble of randomly oriented particles.

For spherical particles, we use Mie-theory and for nonspherical ice crystal particles, GO approximation to calculate the scattering matrix [12,13].

C. Combined Method for Fast Radiative Transfer Simulations in Absorption Bands Including Polarization

The disadvantage of accurate line-by-line radiative transfer simulations for gaseous absorption bands is the time consumption of such codes, especially if taking polarization into account. To overcome this drawback we combine two methods to significantly improve the calculation time, while maintaining a high accuracy compared to line-by-line simulations.

For the monochromatic multiple scattering simulations of polarized light in a vertically inhomogeneous atmosphere, we use the doubling-adding method (DAK—doubling-adding KNMI) [14–16] and combine this with the k-binning method, which is similar to a k-distribution approach, but overcomes shortcomings of a conventional k-distribution [6,7]. The idea of a conventional k-distribution method is to put absorption lines, within a certain wavelength interval, in order of absorption strength rather than of wavelength, resulting in a smooth dependence of absorption coefficient. This, in turn, makes spectral integration much easier and less time consuming. This is done for each channel of a given instrument. The significant difference between k-binning and a conventional k-distribution is that the entire absorption band is simulated and afterward the radiances for each channel are reconstructed from the simulations that represent the entire spectral band. Thus no assumptions about the shape of the sensor weighting function have to be considered *a priori* for a given spectral interval. Any sensor response function can be constructed from a set of radiative transfer simulations for a spectral interval. This requires, to some extent, different constraints on the way the subdivision in spectroscopically similar intervals is performed. It has to be ensured that not only the band-averaged transmission is resembled to high accuracy, but also the transmission in each spectroscopically similar k-binning interval.

In the following we outline our combined method for fast simulations of radiance and polarization in absorption bands:

Step 1: k-binning. We calculate the molecular absorption coefficient k_i (or molecular absorption optical thickness τ_i^{abs}) for the $i = 1, \dots, N$ k-binning intervals and each atmospheric layer using the k-binning method. As molecular spectroscopic database we used HITRAN 2001 [17]. The sensor’s spectral response function $f(\lambda)$ is not considered *a priori*, instead the entire spectral band is subject to the k-binning analysis. The number of resulting k-binning intervals depends on the considered band interval, the resolution steps with which k-binning samples the spectroscopic database, the band-averaged transmission accuracy, and the transmission accuracy in each spectroscopically similar k-binning interval. Resulting k-terms $k_i(\gamma)$ are no longer in the wavelength space, but rather in the Γ space, in which the wavelengths are sorted in order of increasing

gas absorption coefficient $k(\lambda)$. There is a bijective mapping function between λ and γ with $B(\lambda) = \gamma$ and $B^{-1}(\gamma) = \lambda$. This function is called the index function and maps from wavelength space into Γ space.

Step 2: Mie/GO calculations. We calculate the single scattering properties of the atmospheric scatterers (aerosols, cirrus clouds) at given wavelength λ_c using Mie-theory and/or the GO approximation (see also Subsections 2.B and 3.A). Wavelength λ_c is used for the monochromatic radiative transfer simulations following in Steps 3 and 4.

Step 3: DAK calculations. We use DAK to calculate the molecular scattering properties (molecular scattering coefficient σ_{sca} or molecular scattering optical thickness τ_{sca} and the depolarization factor δ) at λ_c . The scattering properties are assumed to be constant over the entire band. Chosen wavelength λ_c lies within the absorption band and stays constant throughout the calculations, e.g., 765 nm if considering the O₂A band. Subsequent to the calculations of the molecular scattering properties, we use DAK for the monochromatic multiple scattering simulations of the Stokes vector \mathbf{I}_i for the $i = 1, \dots, N$ k-binning intervals, in which the underlying surface is assumed to be Lambertian, and thus the reflected light is assumed to be unpolarized and isotropic.

Step 4: Weighting. We calculate the components of the Stokes vector \mathbf{I} for arbitrary instrument channels within the considered band. Considering the results above and instrument response function $f(\lambda)$, we only have to know how much each k-binning interval i contributes to the total spectral response of the channel. This fraction can be calculated by

$$w_i = \int_{\Delta\gamma_i} f(B^{-1}(\gamma)) d\gamma. \quad (5)$$

The weights constitute the weighting of an instrument channel with response function $f(\lambda)$ in the k-binning. Now the components of the Stokes vector \mathbf{I} of this channel can be constructed using

$$\mathbf{I} = \sum_{i=1}^N w_i \mathbf{I}_i, \quad (6)$$

where \mathbf{I} is the Stokes vector of the designated instrument channel and \mathbf{I}_i are the results of the monochromatic radiative transfer simulations for the $i = 1, \dots, N$ k-binning intervals. For example, if one particular channel is fully within one k-binning interval, e.g., an absorption-free channel, the corresponding weight $w_i = 1$. From this consideration it is obvious that not only the broad-band transmission, but also the transmission within each k-binning interval, has to be accurate.

This approach significantly reduces the number of necessary simulations for different sensors and therefore reduces the computational cost.

D. Error Estimation of the Combined Method

In this subsection we show the error in Stokes component I and P_s of transmitted and reflected light within the O₂A band between 755 and 775 nm, using the combined method. We determine the error by comparing intensity I^{lbl} and the degree of linear polarization P_s^{lbl} as calculated using the line-by-line method, with I^{com} and P_s^{com} calculated using the combined method. We used a spectral response function with a resolution of 0.36 nm at FWHM and an equal spacing of 0.21 nm, which is similar to satellite spectrometers such as the Global Ozone Monitoring Experiment (GOME and GOME-2) or the scanning imaging absorption spectrometer for atmospheric cartography (SCIAMACHY) [18,19]. The error of the degree of linear polarization is defined as

$$\varepsilon_P = P_s^{\text{com}} - P_s^{\text{lbl}} \quad (7)$$

and the error of I as

$$\varepsilon_I = (I^{\text{com}} - I^{\text{lbl}})/I^{\text{lbl}}. \quad (8)$$

Here the superscripts “com” and “lbl” refer to the combined method and the line-by-line method, respectively.

The line-by-line calculations of I and P_s for diffusely transmitted and reflected light are performed using DAK at a solar zenith angle of $\theta_0 = 65^\circ$, a viewing zenith angle of $\theta = 0^\circ$, a spectral resolution of 0.01 nm, a surface albedo of $A_s = 0.2$, and a standard midlatitude summer atmosphere. In addition to molecular Rayleigh scattering we assume two types of aerosols, aerosol₁ and aerosol₂; see Table 1. The aerosols are located in the boundary layer (0–1 km). In the case of aerosol₁ the optical thickness is $\tau = 0.048$, resembling clear sky conditions, and in the case of aerosol₂ $\tau = 0.350$, resembling hazy sky conditions. Figure 2 shows line-by-line calculations and convoluted spectra of the transmitted radiance and degree of linear polarization in the O₂A band. For the error analysis, we use the results obtained using aerosol₁. In this case the diffuse transmission is lower, compared to aerosol₂, which results in a higher sensitivity of the error to small differences between the line-by-line and the combined method calculations.

For the combined method calculations we used 37 k-binning intervals, thus reducing the calculation time by a factor of 54, as compared to the line-by-line calculations. For further k-binning input parameters, see Table 3.

Figures 3(a) and 3(b) show results of the convoluted line-by-line and the combined method for I and P_s for transmitted light as a function of wavelength λ , at $\theta_0 = 65^\circ$ and $\theta = 0^\circ$. Figures 3(c) and 3(d) show errors ε_I and ε_P for transmitted light as a function of wavelength λ . Figures 3(e) and 3(f), on the other hand, show errors ε_I and ε_P for reflected light as a function of wavelength λ . The largest errors in I and P_s occur around $\lambda = 760$ nm, where we find

Table 1. Aerosol Model Parameters Used in the Radiative Transfer Simulations^a

Aerosol Parameter	Symbol	Aerosol ₁ (clear sky)	Aerosol ₂ (hazy sky)
Wavelength	λ [μm]	0.765	0.765
Imaginary part of the refractive index	m_i	0.0000	0.0007
Real part of the refractive index	m_r	1.400	1.380
Median radius of the fine mode	r_f [μm]	0.080	0.120
Median radius of the coarse mode	r_c [μm]	0.425	0.700
Standard deviation of the fine mode	σ_f	1.300	1.950
Standard deviation of the coarse mode	σ_c	2.200	2.200
Weighting factor of the fine mode	w	0.9996	0.9992

^aThe spherical aerosol types are representative for clear and hazy sky conditions in the Netherlands [20].

strong absorption [Figs. 3(c)–3(f) (solid line)]. For transmission, the error in the degree of linear polarization is $\epsilon_P \leq 0.11\%$ and in the radiance $\epsilon_I \leq 3.1\%$, while for reflection, the error in the degree of linear polarization is $\epsilon_P \leq 0.31\%$ and in the radiance $\epsilon_I \leq 3.1\%$. The errors in the degree of linear polarization are an order of magnitude smaller than in the radiance. Since P_s is a relative result, see Eq. (3), it appears that the errors in I and Q largely cancel each other.

To further increase the accuracy of the combined method we can increase the number of k-binning intervals for the chosen band interval, or we can limit the simulations to individual channels of the chosen instrument.

Furthermore, a slope occurs in ϵ_I and ϵ_P , which can be explained as follows: In the combined method, as outlined in Subsection 2.C, we use constant wavelength λ_c for the calculations, which should be representative for the whole absorption band. This assumes that the scattering properties of the atmosphere are wavelength independent within the absorption band. Apparently this assumption does not apply for the whole absorption band as can clearly be seen in the spectral slope of ϵ_I and ϵ_P [see Figs. 3(c), 3(d), and 3(f)]. The slope of ϵ_I in

Fig. 3(e) is less pronounced. Still we find a pronounced slope in ϵ_P [see Fig. 3(f)]. This is caused by a slope occurring in Q , not shown here.

To overcome this problem we apply the following solution: Let λ_1 , λ_2 , and λ_3 be three wavelengths that all have contributions from one particular k-binning interval. In its current form k-binning will pick one of them, e.g., λ_2 as a representative for all three. But if the scattering properties are wavelength dependent, the actual components of Stokes vector \mathbf{I} at λ_3 will not be equal to the one at λ_2 . Assuming that the scattering optical thickness exhibits a linear spectral behavior for the absorption band, we can find the minimum and maximum wavelengths where a certain k-binning interval contributes to the radiance, in this case λ_1 and λ_3 . Now we simulate the k-binning interval at λ_1 and λ_3 , not only at λ_2 as done previously. Let the outcome be $\mathbf{I}(\lambda_1)$ and $\mathbf{I}(\lambda_3)$. To get the components of Stokes vector $\mathbf{I}(\lambda_2)$, we interpolate linearly in λ between $\mathbf{I}(\lambda_1)$ and $\mathbf{I}(\lambda_3)$.

The above can potentially be done with all k-binning intervals that cover a wide spectral range, which would double the calculation time. Applying this to 2–5 intervals that have the least absorption we already solve the problem of the wavelength dependency; see the corrected slopes in Fig. 3.

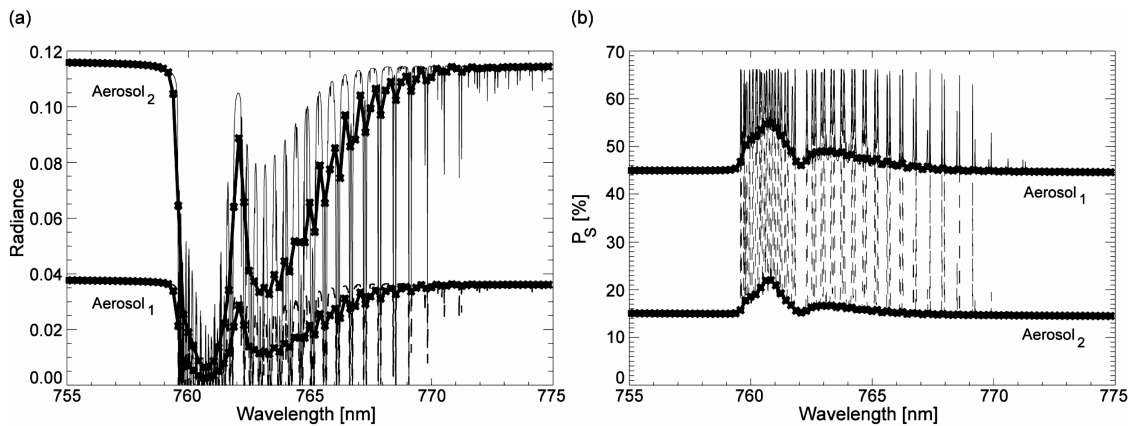


Fig. 2. Simulations of the O₂A band as a function of wavelength for the zenith sky at a solar zenith angle of $\theta_0 = 65^\circ$ for different aerosol types (see Table 1) using line-by-line calculations with a spectral resolution of 0.01 nm (thin lines), and the spectrum convolved using a slit function with a spectral resolution of 0.36 nm at FWHM and an equal spacing of 0.21 nm (thick lines). The aerosol is located in the BL of the atmosphere with an aerosol optical thickness of $\tau_{BL} = 0.048$ in the case of Aerosol₁ and $\tau_{BL} = 0.350$ in the case of Aerosol₂. The asterisk (*) indicates the convolved spectrum. The surface albedo is $A_s = 0.20$. (a) Transmitted radiance. (b) Degree of linear polarization P_s of transmitted light.

3. Sensitivity of the Degree of Linear Polarization of the Zenith Skylight in the O₂A Band to Aerosol Altitude

In this section, we analyze the sensitivity of the degree of linear polarization of the zenith skylight in the spectral region of the O₂A band to changes of aerosol altitude, aerosol microphysics, and aerosol optical thickness τ_{aer} in the troposphere and lower stratosphere. For the simulations we used the combined method, which combines both a high accuracy ($\varepsilon_P \leq 0.11\%$) and short computing time. We used a spectral response function with a resolution of 0.36 nm at FWHM and an equal spacing of 0.21 nm. Throughout this study we use two different types of atmospheric scatterers, namely spherical aerosols according to Mie scattering theory and nonspherical ice crystal particles according to the GO approximation method. If not mentioned otherwise, the viewing geometry is as follows: solar zenith angle $\theta_0 = 65^\circ$ and viewing zenith angle $\theta = 0^\circ$. The microphysical properties of the spherical aerosol particles were derived from actual measurements at clear sky conditions (aerosol₁) and hazy sky conditions (aerosol₂) taken in Cabauw, the Netherlands (see Table 1) [20]. The microphysical properties of the nonspherical ice crystals correspond to C_1 imperfect hexagonal ice crystals (IMP), which are randomly oriented (see Table 2) [13,21]. The tilt angle α , which can be considered as the degree of the distortion of the surface of the ice crystals, is set to 30° . For this choice of tilt angle the phase function varies rather smoothly with the scattering angle and does not show the sharp angular features of a pristine hexagon phase function, e.g., halo peaks. This tilt angle value is suitable for the representation of natural (irregular) ice crystals in clouds. The size of a hexagonal crystal is given by its length L and so-called radius r . Depending on the magnitude of the aspect ratio ($L/2r$), the crystal is a column ($L/2r > 1$) or a plate ($L/2r < 1$). Effective radius r_{eff} of the ice crystal is defined here as the radius of a sphere that has the same volume as the hexagon:

$$r_{\text{eff}} = \left(\frac{9\sqrt{3}}{8\pi} r^2 L \right)^{1/3}. \quad (9)$$

Table 2. Ice Crystal Model Parameters Used in the Radiative Transfer Simulations^a

Ice Crystal Parameter	Symbol	Ice Crystal C_1
Wavelength	λ [μm]	0.765
Imaginary part	m_i	0.783E-07
Real part	m_r	1.306
Length	L [μm]	30
Radius	R [μm]	10
Effective radius	r_{eff} [μm]	12.2997
Aspect ratio		1.5
Orientation		random

^aThe imperfect hexagonal ice crystal C_1 represents cirrus cloud particles [21].

Figure 4 shows calculations of phase function F_{11} and single scattering polarization $-F_{12}/F_{11}$ for all three types of scatterers. As expected, we find higher polarization for the small aerosol type, compared to the large aerosol and ice crystals [20,21].

A. Processes Determining the Degree of Linear Polarization in the O₂A Band

For a general interpretation of the processes that determine the degree of linear polarization in the O₂A band we consider four processes that account for Stokes vector elements I and Q and the resulting degree of linear polarization P_s of the cloud free sky: (1) single scattering in the atmosphere (either by molecules or aerosols); (2) direct transmission to the surface, subsequent reflection by the depolarizing surface, and single scattering in the atmosphere; (3) multiple scattering in the atmosphere; and (4) higher order surface reflection and atmospheric scattering. These four processes provide the contributions to skylight measurements.

To understand the role of these processes we analyze, below, the influence of molecular scattering, aerosol scattering, surface albedo, aerosol altitude, and vertical distribution of aerosols on the degree of linear polarization in the O₂A band (see Fig. 5):

a. Molecular scattering, $A_s=0.00$ [Fig. 5 (solid line)]: For a purely Rayleigh scattering atmosphere we find a high degree of linear polarization in the

Table 3. K-Binning Parameters

K-Binning Parameter	Symbol	Input
Atmospheric profile		Midlatitude Summer, AFGL (1986)
Filter function		rectangular
Minimum wavelength ^a	[nm]	755
Maximum wavelength ^a	[nm]	775
Wavelength resolution ^b	[nm]	0.01
Threshold ^c	[%]	0.01/(0.005)
Maximum error ^d	[%]	0.001
Intervals needed		37

^aThe minimum and maximum wavelengths define the spectral region under consideration.

^bThe wavelength resolution specifies the resolution with which the spectral database is sampled.

^cThe threshold refers to the user defined threshold for the total atmospheric transmittance error. The value in brackets refers to the additional threshold applied to the atmospheric transmission error for each layer.

^dThe maximum error refers to the maximum error of the atmospheric transmittance in each of the k-binning intervals [6,7].

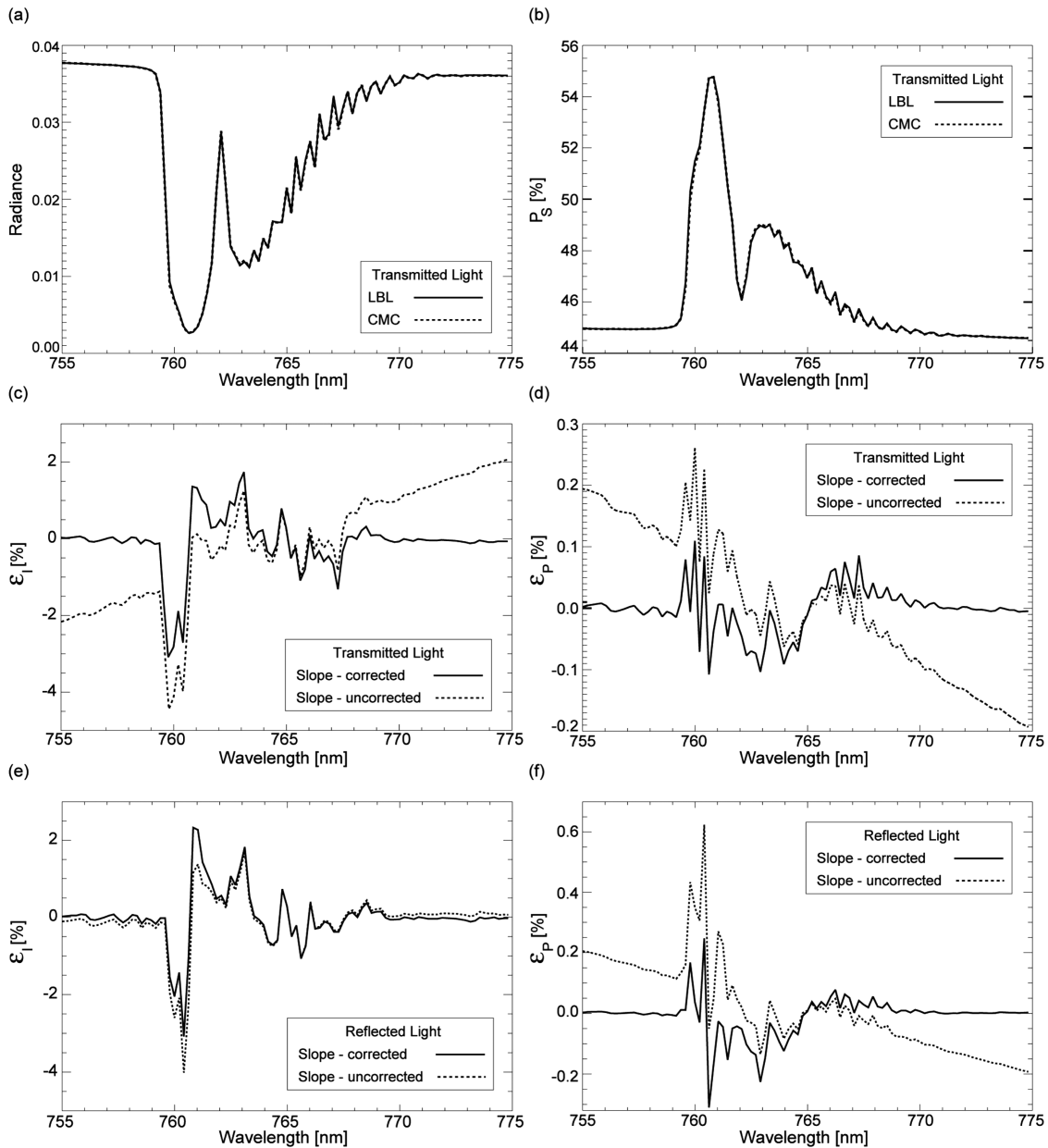


Fig. 3. Comparison of line-by-line (LBL) and combined method calculations (COM) of radiance and degree of linear polarization P_s within the O_2A band as a function of wavelength for zenith/nadir view at a solar zenith angle of $\theta_0 = 65^\circ$. The surface albedo is $A_s = 0.20$. The BL contains $Aerosol_1$ with $\tau_{BL} = 0.048$. (a) Transmitted radiance of zenith skylight. (b) Degree of linear polarization of the zenith skylight. (c) Error of the transmitted radiance ϵ_I [see Eq. (8)]. The dotted line shows ϵ_I without slope-correction and the solid line with slope-correction. (d) Error of the degree of linear polarization of the zenith skylight ϵ_P [see Eq. (7)]. The dotted line shows ϵ_P without slope-correction and the solid line with slope-correction. (e) As in (c), but for reflected light at top-of-the-atmosphere in nadir view. (f) As in (d), but for reflected light in nadir viewing direction.

continuum due to scattering by strongly polarizing molecules. Since the Rayleigh optical thickness at 765 nm is only 0.0255 there is not much multiple scattering in the continuum. However, inside the O_2A band the small amount of multiple scattering is further reduced by means of absorption. Therefore we find a slightly higher degree of linear polarization inside the absorption band (P_b), as compared to the continuum (P_c).

b. Molecular and aerosol scattering, $A_s=0.00$ [Fig. 5 (dotted line)]: Adding weakly polarizing aerosols with $\tau_{aer} = 0.10$ to the boundary layer (0–1 km)

strongly decreases P_c , while P_b decreases less strongly. The decrease of P_c is stronger for higher aerosol optical thicknesses (increase of multiple scattering). Inside the O_2A band, light is mainly scattered at higher altitudes because the strong gaseous absorption prevents light to reach lower parts of the atmosphere; thus molecular scattering dominates polarization inside the O_2A band, which results in a higher P_b .

c. Molecular and aerosol scattering, $A_s=0.02$ [Fig. 5 (dashed line)] and 0.20 [Fig. 5 (dash-dotted line)]: Adding surface reflection with a low albedo

of $A_s = 0.02$ (resembling water surfaces) shows little effect on P_c and nearly no effect on P_b . Inside the absorption band the surface is shielded due to the gaseous absorption and this causes the lower effect on P_b . Increasing the surface albedo to $A_s = 0.20$ we see a further decrease of P_c and P_b . In these cases the decrease of the degree of linear polarization is mainly because the atmosphere is bounded by a depolarizing Lambertian surface. Increasing surface reflection decreases the degree of linear polarization because I increases and Q remains unchanged. The decrease in P_s is more pronounced for small solar zenith angles. This increase of surface influence with smaller solar zenith angles is due to the more efficient transmission of the direct beam through the atmosphere and the consequently stronger illumination of the surface. At the same time, the more efficient transmission causes less multiple scattering [22]. Inside the O_2A band the surface is shielded due to the gaseous absorption.

d. As (c), but increasing the aerosol layer altitude [Fig. 5 (dashed double dotted line)]: An altitude increase from 1 to 16 km of the aerosol layer shows a negligible influence on P_c , whereas the influence on P_b is strong. The influence of aerosol altitude on P_b is due to the strong O_2A -band absorption, which prevents light to reach lower parts of the atmosphere. Because most of the sunlight inside the absorption band is scattered at higher altitudes, an increase in aerosol altitude increases the probability of aerosol scattering as compared to molecular scattering and is thus decreasing P_b . For weakly polarizing aerosols this can lead to a band polarization that is lower than the continuum polarization. Whereas in the continuum, sunlight can interact with all scatterers in the entire atmosphere, provided that the scatterers are nonabsorbing and that the optical thickness of the scatterers is below about 1. Inside the band, as a result of the strong absorption, sunlight only interacts with the upper part of the atmosphere. Aerosol absorption affects molecular scattering below the aerosol layer, and the underlying Rayleigh scattering produces only a small signal.

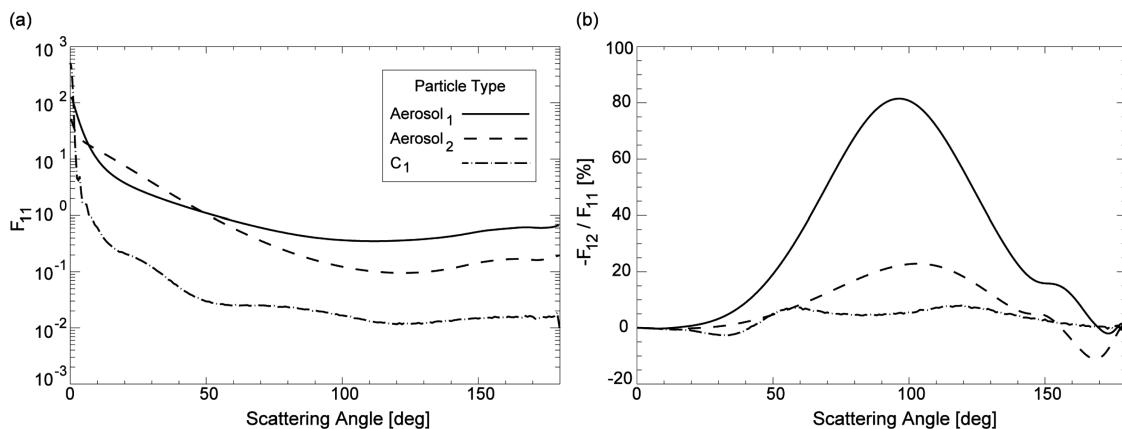


Fig. 4. Scattering matrix elements F_{11} and $-F_{12}/F_{11}$ as computed at $\lambda = 765$ nm for different types of scatterers (see Tables 1 and 2). Mie-theory was used for the simulations of the spherical aerosols and the GO approximation method for the nonspherical ice crystal. (a) Phase function F_{11} as a function of scattering angle. (b) Single scattering polarization $-F_{12}/F_{11}$ as a function of scattering angle.

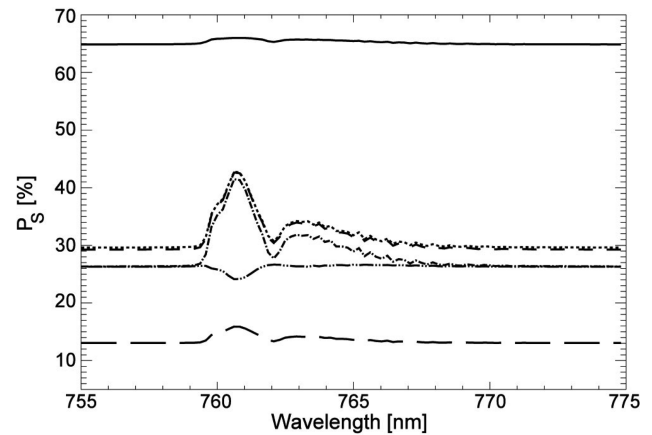


Fig. 5. Degree of linear polarization of zenith skylight as a function of wavelength at a solar zenith angle of $\theta_0 = 65^\circ$ showing processes that determine the polarization in the O_2A band: pure Rayleigh scattering (solid line) without surface reflection; inclusion of Aerosol₂ to the boundary layer with a geometric thickness of 1 km and an optical thickness of 0.1 (dotted line); adding a surface albedo of $A_s = 0.02$ (dashed line) and of $A_s = 0.20$ (dash-dotted line); elevation of the aerosol layer up to 16 km (dashed double dotted line); and inclusion of Aerosol₂ to the boundary layer with an optical thickness of 0.35 (long dashed line).

In that case we find a small decrease of P_c with increasing aerosol altitude.

e. As (d), but adding a second aerosol layer [Fig. 5 (long dashed line)]: Adding a second aerosol layer between 0 and 1 km with weakly polarizing aerosol having an optical thickness of $\tau_{aer} = 0.35$ increases multiple scattering and further decreases the degree of linear polarization of P_c and P_b , as in process (b). Adding a second scattering layer can strongly alter the effect of process (d), depending on the single scattering properties and aerosol optical thickness of the added layer. This is studied in the next subsection.

B. Simulations of the Effect of Aerosol Altitude on the Degree of Linear Polarization of the Zenith Skylight

In this section we study the influence of aerosol altitude, microphysical properties, and aerosol optical

thickness changes on the degree of linear polarization P_s within the O_2A band. This is done for different types of model atmospheres (see Fig. 6). The basic atmosphere is a Rayleigh scattering atmosphere with oxygen as the only absorbing gas. In this atmosphere we place a boundary layer (BL), which comprises aerosols, and/or an elevated layer (EL), which comprises aerosols or ice crystals (see Table 1 and 2). The boundary layer is located between 0 and 1 km. The aerosol optical thickness of the boundary layer is $\tau_{BL} = 0.048$, resembling clear sky conditions, or $\tau_{BL} = 0.350$, resembling hazy sky conditions. The elevated layer, with a geometric thickness of 1 km, is shifted through the atmosphere in steps of 2 km. The optical thickness of the elevated layer is $\tau_{EL} = 0.03$ or $\tau_{EL} = 0.10$. Referring to C_1 ice crystals this resembles a range from subvisible to thin cirrus clouds [23]. The surface albedo is chosen to be $A_s = 0.20$.

1. Basic Atmosphere Plus an Elevated Scattering Layer

Figure 7(a) shows P_s as a function of wavelength for the basic model atmosphere with an added scattering layer at different altitudes and for different types of scatterers. The aerosol optical thickness of the elevated layer is $\tau_{EL} = 0.10$. Furthermore, we included P_s for pure Rayleigh scattering to illustrate the processes (a) and (b) of Subsection 3.A, which describe the effect on P_s by adding aerosol to a Rayleigh atmosphere. To illustrate the influence of aerosol layer altitude changes on the degree of linear polarization in the continuum P_c and within the absorption band P_b in a more pronounced way, we show P_c and polarization difference $P_b - P_c$ as function of the aerosol layer altitude [see Fig. 7(b)]. The polarization inside the O_2A band can be larger or smaller than in the continuum [see Subsection 3.A (d)]. This is indicated by a change of the sign of $P_b - P_c$. The circles in Fig. 7(a) indicate P_c , selected at 757.9 nm and P_b , selected at 760.6 nm. Figure 7(b) shows P_c , marked by

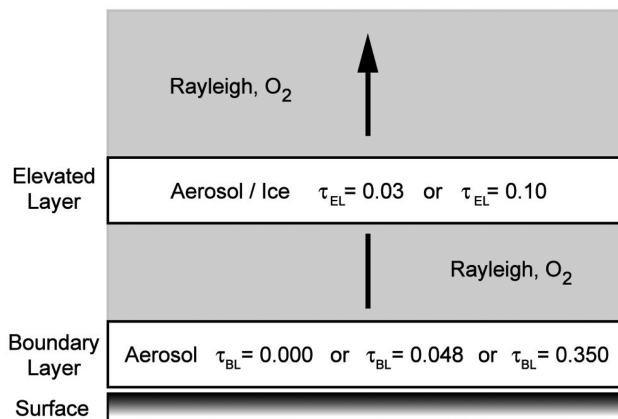


Fig. 6. Schematic representation of the model atmosphere. The model atmosphere comprises molecules, aerosols, and ice crystals (see Tables 1 and 2). The molecules are homogeneously mixed throughout the atmosphere according to the pressure profile, while the aerosols are located within the boundary layer, between 0 and 1 km, and inside an elevated layer. The aerosols in the elevated layer can be replaced by ice crystals and the altitude of the elevated layer is variable between 2 and 16 km. Furthermore, the optical thicknesses of the boundary layer and the elevated layer are variable. The atmosphere is bounded by a Lambertian surface.

an asterisk, and $P_b - P_c$ as a function of altitude for three different types of scatterers. As outlined in Subsection 3.A (d), we find a decrease of P_b with increasing aerosol altitude for all scatterers, while P_c remains nearly unaffected if the scatterer is nonabsorbing. In case of the absorbing aerosol₂, we see a decrease of P_c with increasing aerosol altitude, as outlined in Subsection 3.A (d). We also see that the decrease of P_b is more pronounced for weakly polarizing scatterers, in this case aerosol₂ and C_1 .

2. Basic Atmosphere Plus Boundary and Elevated Scattering Layers

Figure 8 shows P_c and $P_b - P_c$ as a function of aerosol altitude for the basic model atmosphere with an

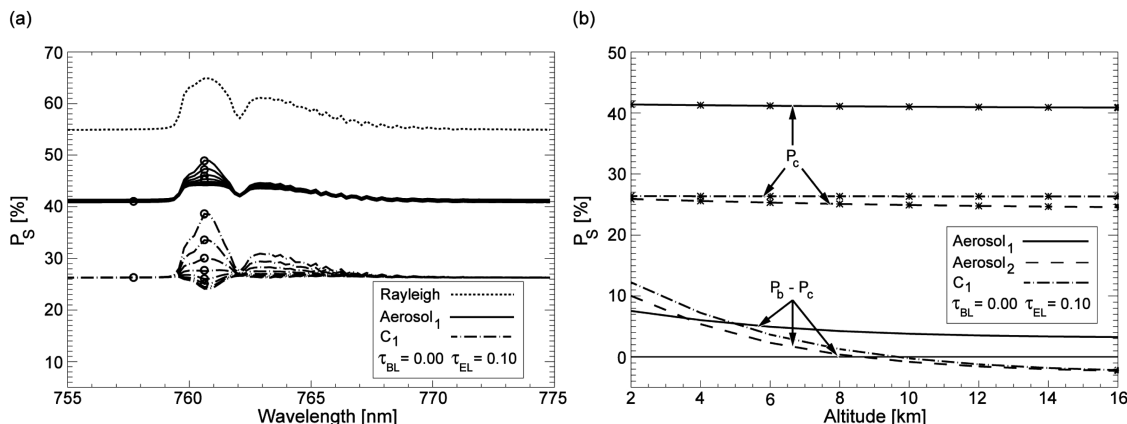


Fig. 7. (a) Degree of linear polarization of the zenith skylight as a function of wavelength at a solar zenith angle of $\theta_0 = 65^\circ$ for a pure Rayleigh atmosphere and for an atmosphere including an elevated scattering layer at different altitudes. The elevated layer contains different types of scatterers, while the boundary layer contains no aerosol. The surface albedo is $A_s = 0.20$. The circles indicate continuum polarization P_c , selected at 757.9 nm, and O_2A band polarization P_b , selected at 760.6 nm. (b) Continuum polarization (asterisk) and difference between band and continuum polarization $P_b - P_c$ as a function of the elevated layer altitude.

added boundary scattering layer and an elevated scattering layer. Both the boundary and the elevated layer contain scatterers of the same type: strongly polarizing aerosol₁ [Figs. 8(a) and 8(b)] and weakly polarizing aerosol₂ [Figs. 8(c) and 8(d)]. In Figs. 8(a) and 8(c) the optical thickness of the boundary layer is $\tau_{BL} = 0.048$ and in 8(b) and 8(d) $\tau_{BL} = 0.350$. Adding the same kind of scatterer in the boundary layer has a similar effect as an increase of the aerosol optical thickness and causes a decrease of P_c and P_b , compared to the case without boundary layer aerosol [see Subsection 3.A (e)]. Furthermore, we show the results for weakly polarizing C_1 ice crystals added to the elevated layer to simulate the influence of cirrus clouds [see Fig. 8(c) and 8(d)]. No sign change of $P_b - P_c$ occurs in the case of weakly polarizing aerosol₂ or C_1 . We find that the influence of the elevated layer altitude on P_b decreases if the aerosol optical thickness of the boundary layer increases. This can be explained as follows: I_b as a function of aerosol layer altitude h can be written as

$$I_b(h) \cong I_{BL,b} + I_{mol,b} + I_{EL,b}(h), \quad (10)$$

where $I_{BL,b}$ is determined by aerosol scattering in the boundary layer, $I_{mol,b}$ is determined by Rayleigh

scattering, and $I_{EL,b}(h)$ is determined by scattering in the elevated layer. Analogously we can write

$$Q_b(h) \cong Q_{BL,b} + Q_{mol,b} + Q_{EL,b}(h). \quad (11)$$

An increase of boundary layer aerosol optical thickness τ_{BL} causes more multiple scattering, which leads to a decrease of P_b , due to a stronger increase of Stokes parameter $I_{BL,b}$ as compared to $Q_{BL,b}$. Assuming that the absolute changes of $\Delta I_{EL,b}$ and $\Delta Q_{EL,b}$ with increasing aerosol layer altitude are independent of changes to τ_{BL} , we find that the relative increase of $I_b(h)$ with increasing altitude of the elevated layer reduces strongly in the case of high τ_{BL} ; while in comparison, the relative increase of $Q_b(h)$ reduces less, as compared to the case of low τ_{BL} . Thus, in the case of high τ_{BL} the degree of linear polarization $P_b = -Q_b/I_b$ decreases less strongly with increasing altitude of the elevated scattering layer than in the case of low τ_{BL} .

Figure 9 shows P_c and $P_b - P_c$ as a function of aerosol altitude for the basic model atmosphere with an added boundary and elevated aerosol layer. In this case the boundary and the elevated layer comprise different types of scatterers: strongly polarizing aerosol₁ in the boundary layer and weakly polarizing

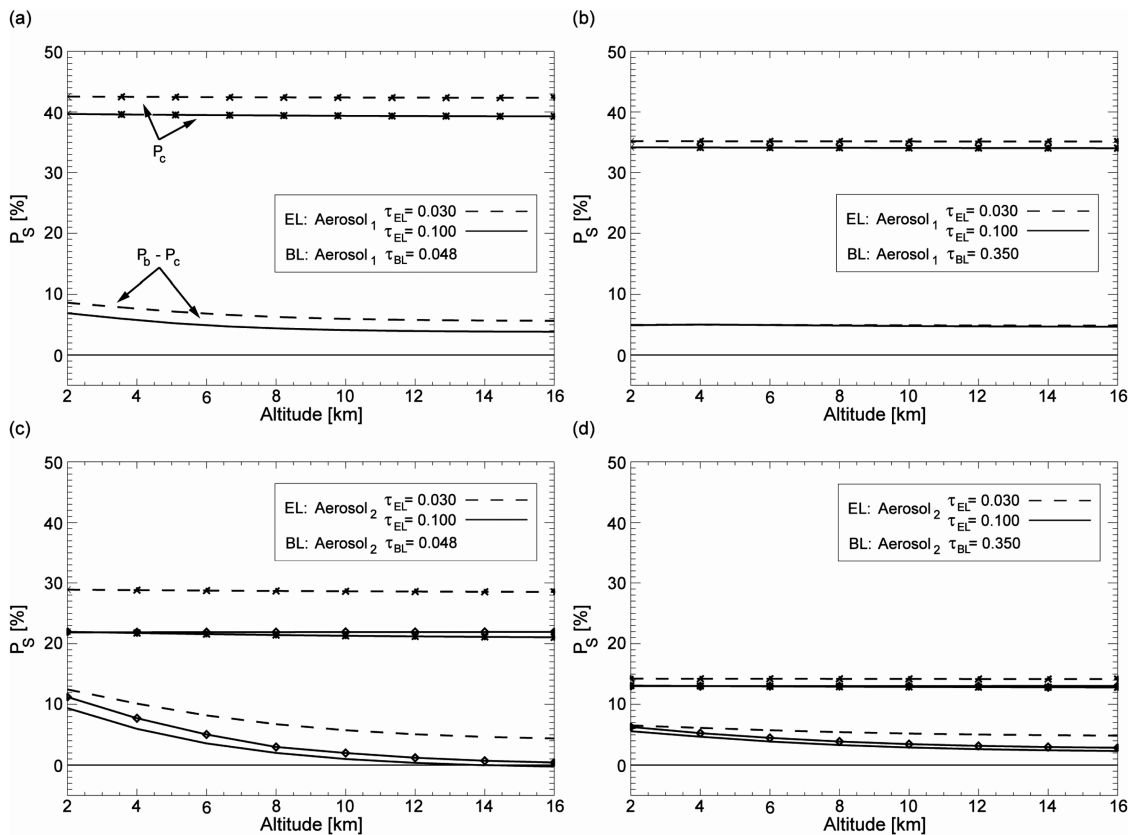


Fig. 8. Continuum polarization P_c (asterisk) and band-continuum polarization $P_b - P_c$ as a function of the elevated layer altitude for zenith skylight at a solar zenith angle of $\theta_0 = 65^\circ$ with a surface albedo of $A_s = 0.20$ and different optical thicknesses of the boundary and elevated layer. The boundary and elevated layers contain aerosols of the same type. The boundary layer optical thickness of $\tau_{BL} = 0.048$ resembles clear sky conditions and a thickness of $\tau_{BL} = 0.350$ resembles hazy sky conditions. (a) and (b) BL and EL comprise Aerosol₁. (c) and (d) BL and EL comprise Aerosol₂. Here we also included results using scatterer C_1 in the elevated layer with an optical thickness of $\tau_{BL} = 0.10$ (denoted by diamonds).

aerosol₂ in the elevated layer [Figs. 9(a) and 9(b)]; weakly polarizing aerosol₂ in the boundary layer and strongly polarizing aerosol₁ in the elevated layer [Figs. 9(c) and 9(d)]. In Figs. 9(a) and 9(c) the optical thickness of the boundary layer is $\tau_{BL} = 0.048$ and in Figs. 9(b) and 9(d) $\tau_{BL} = 0.350$. Adding aerosol scatterers with different polarization properties (see Fig. 4) in the boundary layer can cause an increase as well as a decrease of P_c and P_b , as compared to the basic model atmosphere with only an elevated aerosol layer added (see Fig. 7). Furthermore, we show the results for weakly polarizing C_1 ice crystals added to the elevated layer, to simulate the influence of cirrus clouds [see Figs. 9(a) and 9(b)].

In the case of strongly polarizing aerosol₁ located in the boundary layer and weakly polarizing aerosol₂ or C_1 in the elevated layer, a sign change of $P_b - P_c$ occurs [see Figs. 9(a) and 9(b)]. For low τ_{BL} we see an increase of P_c , while P_b changes less as compared to the basic model atmosphere with only an elevated aerosol layer added. Thus, the sign change of $P_b - P_c$ occurs at lower altitudes and $P_b - P_c$ is lower at higher altitudes. As can be seen in Fig. 8, an increase of τ_{BL} to 0.350 leads to a decrease of P_c and P_b , due to an increase of multiple scattering, and, also, the effect of aerosol altitude is reduced.

In the case of weakly polarizing aerosol₂ located in the boundary layer and strongly polarizing aerosol₁

in the elevated layer, we find that an altitude increase of the elevated layer can also cause an increase in P_b [see Figs. 9(c) and 9(d)]. For low τ_{BL} we find the expected decrease in P_b with increasing altitude of the elevated layer, whereas for high τ_{BL} we find that an altitude increase of the elevated layer causes an increase of P_b instead of a decrease. In the case of strongly polarizing aerosol located in the elevated layer, the absolute change of $\Delta Q_{EL,b}$ is larger and $\Delta I_{EL,b}$ is smaller, as compared to the case with weakly polarizing aerosol located in the elevated layer [Fig. 8(d)]. This leads to a stronger relative increase of Q_b , while the relative change of I_b increases less (see Eqs. (10) and (11)). If τ_{BL} is high enough, the relative increase of Q_b becomes larger than that of I_b , resulting in an increase of P_b with increasing aerosol layer altitude.

Based on the above presented simulations of the influence of aerosol altitude on the degree of linear polarization of the zenith skylight in the O₂A band we may conclude the following, regarding the measurements taken on 11 May 1994 [Fig. 1(a) (solid line)] and on 19 October 1993 [Fig. 1(b) (solid line)]: It seems likely that the observed decrease of P_b inside the O₂A band was caused by a second scattering particle layer in the upper troposphere, probably thin cirrus, since the stratospheric aerosol scattering optical thickness is generally very low, except shortly

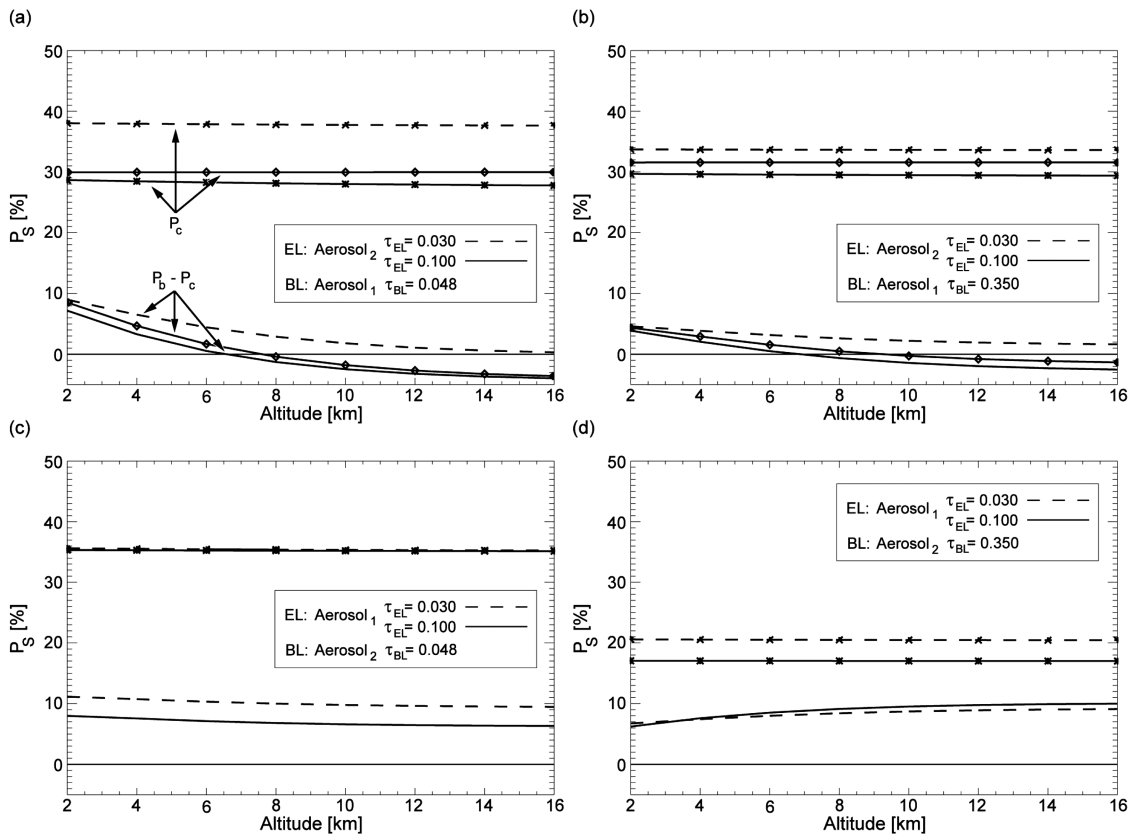


Fig. 9. As in Fig. 8, but now the boundary and elevated layer contain different types of aerosol. (a) and (b) BL comprises Aerosol₁ and EL comprises Aerosol₂; here we also included results using scatterer C_1 in the elevated layer with an optical thickness of $\tau_{BL} = 0.10$ (denoted by diamonds). (c) and (d) BL comprises Aerosol₂ and EL comprises Aerosol₁.

after volcanic events. During the time of the measurements (1993, 1994) the stratospheric optical thickness was still increased due to effects of the Pinatubo eruption ($\tau_{\text{strat}} \leq 0.05$) [24]. However, this alone is unlikely to have caused the observed low P_b but might have influenced the measurements of the degree of linear polarization in this period.

3. Dependence on Solar Zenith Angle and Spectral Resolution

The results shown above pertain to zenith sky observations with $\theta_0 = 65^\circ$. Figure 10 shows P_s as a function of wavelength for different solar zenith angles. For solar zenith angles θ_0 tending towards the zenith (smaller scattering angle Θ), we find a decrease of P_c (see also Fig. 4) [22]. Furthermore, we find that P_b converges toward P_c [1]. The scattering angle difference can be an explanation of the considerably larger differences of $P_b - P_c$ observed by Preusker *et al.* [Fig. 1(a) solid line], as compared to the observations by Stammes *et al.* [Fig. 1(b) solid line]. Furthermore, the results depend on the spectral resolution of the spectrometer (see Fig. 11). A higher resolution provides a more detailed spectral fine-structure in the polarization and thus the polarization effects, as shown in this section, are more pronounced.

4. Conclusions and Outlook

In this paper we studied the influence of aerosol altitude, aerosol microphysics, and aerosol optical thickness on the degree of linear polarization of the zenith skylight in the spectral region of the O₂A band. We developed a combined method for fast radiative transfer simulations in absorption bands including polarization. As a spectral approximation technique we used the k-binning method, and integrated this method in monochromatic doubling-adding multiple scattering calculations. For both reflected and diffusely transmitted light we compared the radiance and the degree of linear polarization as calculated using the combined method with

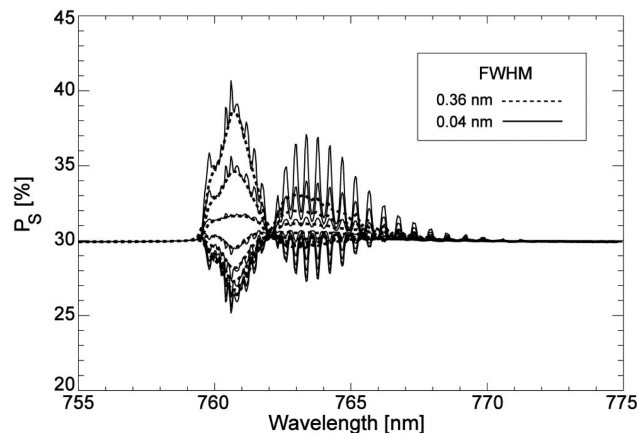


Fig. 11. Degree of linear polarization of zenith skylight as a function of wavelength at a solar zenith angle of $\theta_0 = 65^\circ$ for two different spectral response functions and different altitudes of the elevated scattering layer. The boundary layer comprises Aerosol₁ and optical thickness of $\tau_{BL} = 0.048$ and the elevated layer comprises scatterer C_1 with $\tau_{EL} = 0.100$. The elevated layer is shifted through the atmosphere from 2 to 16 km in steps of two kilometers, resulting in a decrease of P_b with increasing altitude of the elevated layer.

the results of accurate line-by-line simulations. Furthermore, we corrected for the spectral dependency of the scattering properties within the O₂A band. Based on the comparison we conclude that the radiance error due to the assumptions of the k-binning approach is smaller than 3.1% for both the reflected and the transmitted radiation. For the degree of linear polarization, this error is smaller than 0.31% for reflected light and smaller than 0.11% for transmitted light. These maximum errors hold for instrument channels around 760 nm. The errors are smaller for other instrument channels.

Regarding the sensitivity of the degree of linear polarization of the zenith skylight within the O₂A band to changes of aerosol altitude and aerosol optical thickness, we can conclude the following: Increasing the altitude of an elevated aerosol layer within a

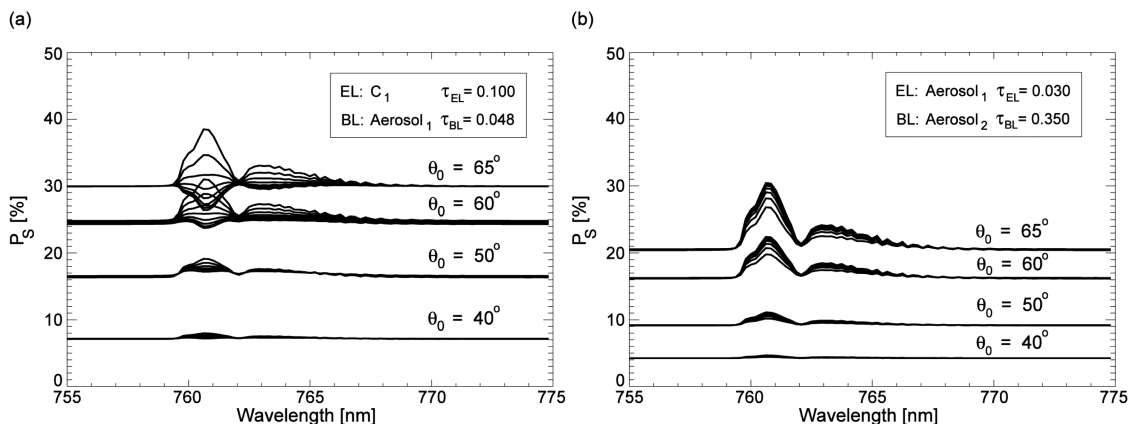


Fig. 10. Degree of linear polarization of zenith skylight as a function of wavelength for different solar zenith angles θ_0 and different altitudes of the elevated scattering layer. The elevated layer is shifted through the atmosphere from 2 to 16 km in steps of two kilometers. The surface albedo is $A_s = 0.20$. (a) BL comprises Aerosol₁ and EL comprises C_1 . P_b decreases with increasing altitude of the elevated layer. (b) BL comprises Aerosol₂ and EL comprises Aerosol₁. P_b increases with increasing altitude of the elevated layer.

Rayleigh scattering atmosphere decreases the degree of linear polarization inside the oxygen absorption band for all scatterers under consideration. The magnitude of this effect depends on the polarization properties of the chosen aerosol or ice crystal. Adding another scattering layer (boundary layer), including aerosols of the same type, decreases the sensitivity of P_b to changes of the scattering layer altitude. A strongly polarizing scatterer in the boundary layer and a weakly polarizing scatterer in the elevated layer increases the sensitivity of P_b to changes of the scattering layer altitude. A weakly polarizing scatterer in the boundary layer and a strongly polarizing scatterer in the elevated layer decreases the sensitivity of P_b to changes of the scattering layer altitude. The higher the optical thickness of the boundary layer, the less sensitive P_b is to changes of the scattering layer altitude. In the case of weakly polarizing aerosol in the boundary layer and strongly polarizing aerosol in the elevated layer, we find an increase of P_b with increasing scattering layer altitude. The sensitivity of P_b to changes of the scattering layer altitude is strongest inside the troposphere and decreases with increasing altitude. The polarization inside the O_2A band can be larger or smaller than the continuum polarization. In the absence of boundary layer aerosols $P_b < P_c$ is only observed for weakly polarizing aerosols or ice crystals within the troposphere and lower stratosphere. In the presence of boundary layer aerosol, we find this effect only for a combination of strongly polarizing scatterers located in the boundary layer together with weakly polarizing scatterers in an elevated scattering layer. For all other cases we find that $P_b < P_c$. Decreasing the optical thickness of the elevated scattering layer decreases the scattering altitude effect on P_b . The polarization in the continuum and inside the absorption band strongly depends on the viewing geometry.

We may tentatively conclude that a retrieval of the aerosol profile from ground-based measurements of the polarization of the cloud free zenith sky in the O_2A -band region seems too ambitious in the case of multiple aerosol layers without additional information on the microphysical aerosol properties and optical thickness of the individual layers. Only in the case of a single aerosol layer, a determination of the aerosol layer altitude may be obtained due to the fact that the retrieval of microphysical aerosol properties and optical thickness is achievable from the continuum. The detection of the presence of a second aerosol or ice crystal layer from polarization measurements might be possible as well. Polarization measurements at a high-altitude site or airplane-based measurements might offer altitude information on aerosols or subvisible cirrus in the upper troposphere/lower stratosphere.

Based on this study of ground-based polarization observations we expect that it is also necessary to include the effect of aerosol altitude in simulations of top-of-the-atmosphere radiance and polarization in

absorption bands. The influence of aerosol altitude and other aerosol properties on the degree of polarization inside gaseous absorption bands will affect the measurements of polarization sensitive spectrometers such as the medium resolution imaging spectrometer (MERIS) [25], the GOME [26–28], the SCIAMACHY [29–31], the polarization and directionality of the Earth's reflectance (POLDER) [32,33], or the upcoming aerosol polarimeter sensor (APS) [34], and the Orbiting Carbon Observatory (OCO) [35–37]. In the near future we plan to apply our method to OCO to study the aerosol influence on the polarization of oxygen and carbon dioxide absorption bands, as observed from space.

We acknowledge the support of the Royal Netherlands Meteorological Institute (KNMI) for funding of part of the work reported here. We thank Daphne M. Stam and Ilse Aben for providing their unique ground-based polarization measurements and for their helpful suggestions on an earlier version of this paper. We also thank Ping Wang for the enhancements of the radiative transfer code.

References

1. P. Stammes, F. Kuik, and J. F. De Haan, "Atmospheric polarization in the oxygen A and B bands," in *Proceedings of Progress in Electromagnetic Research Symposium (PIERS)*, B. Arbesser-Rastburg *et al.*, eds. (Kluwer Academic, 1994), pp. 2255–2259. ISBN: 0-7923-3019-6
2. R. Preusker, U. Boetger, and J. Fischer, "Spectral and bidirectional measurements of the Stokes vector in the O_2A band and their interpretation," *Proc. SPIE* **2582**, 13–20 (1995).
3. I. Aben, F. Helderma, D. M. Stam, and P. Stammes, "High-spectral resolution polarization measurements of the atmosphere with the GOME-BBM," *Proc. SPIE* **3121**, 446–453 (1997).
4. I. Aben, F. Helderma, D. M. Stam, and P. Stammes, "Spectral fine-structure in the polarisation of skylight," *Geophys. Res. Lett.* **26**, 591–594 (1999).
5. D. Stam, J. F. De Haan, J. W. Hovenier, and P. Stammes, "The degree of linear polarization of light emerging from the cloudless atmosphere in the O_2A band," *J. Geophys. Res.* **104**, 16843–16858 (1999).
6. R. Bennartz and R. Preusker, "k-binning: a new approach to simulate narrow band satellite channels in layered atmospheres with variable gas absorption," submitted to *J. Quant. Spectrosc. Radiat. Transfer* (2007).
7. R. Bennartz and J. Fischer, "A modified k-distribution approach applied to narrow band water vapour and oxygen absorption estimates in the near infrared," *J. Quant. Spectrosc. Radiat. Transfer* **66**, 539–553 (2000).
8. S. Chandrasekhar, *Radiative Transfer* (Dover, 1960).
9. H. C. van de Hulst, *Light Scattering by Small Particles* (Dover, 1981).
10. W. A. Shurcliff, *Polarized Light* (Harvard U., 1962).
11. J. W. Hovenier, C. Van der Mee, and H. Domke, *Transfer of Polarized Light in Planetary Atmospheres* (Kluwer, 2004).
12. W. A. De Rooij, and C. A. H. van der Stap, "Expansion of Mie scattering matrices in generalized spherical functions," *Astron. Astrophys.* **131**, 237–248 (1984).
13. M. Hess, R. B. A. Koelemeijer, and P. Stammes, "Scattering matrices of imperfect hexagonal ice crystals," *J. Quant. Spectrosc. Radiat. Transfer* **60**, 301–308 (1998).

14. J. F. De Haan, P. B. Bosma, and J. W. Hovenier, "The adding method for multiple scattering calculations of polarized light," *Astron. Astrophys.* **183**, 371–391 (1987).
15. P. Stammes, "Spectral radiance modelling in the UV-visible range," in *IRS 2000: Current Problems in Atmospheric Radiation*, W. L. Smith and Y. M. Timofeyev, eds. (Deepak, 2001), pp. 385–388.
16. P. Stammes, J. F. De Haan, and J. W. Hovenier, "The polarized internal radiation field of a planetary atmosphere," *Astron. Astrophys.* **225**, 239–259 (1989).
17. L. S. Rothman, A. Barbe, D. C. Benner, L. R. Brown, C. Camy-Peyret, M. R. Carleer, K. Chance, C. Clerbaux, V. Dana, V. M. Devi, A. Fayt, J.-M. Flaud, R. R. Gamache, A. Goldman, D. Jacquemart, K. W. Jucks, W. J. Lafferty, J.-Y. Mandin, S. T. Massie, V. Nemtchinov, D. A. Newnham, A. Perrin, C. P. Rinsland, J. Schroeder, K. M. Smith, M. A. H. Smith, K. Tang, R. A. Toth, J. Van der Auwera, P. Varanasi, and K. Yoshino, "The HITRAN molecular spectroscopic database: edition of 2000 including updates through 2001," *J. Quant. Spectrosc. Radiat. Transfer* **82**, 5–44 (2003).
18. J. P. Burrows, M. Weber, M. Buchwitz, V. Rozanov, A. Ladstätter-Weissenmayer, A. Richter, R. DeBeek, R. Hoogen, K. Bramstedt, K. U. Eichmann, M. Eisinger, and D. Perner, "The global ozone monitoring experiment (GOME): mission concept and first scientific results," *J. Atmos. Sci.* **56**, 151–175 (1999).
19. H. Bovensmann, J. P. Burrows, M. Buchwitz, J. Frerick, S. Noel, V. V. Rozanov, K. V. Chance, and A. P. H. Goede, "SCIAMACHY: mission objectives and measurement modes," *J. Atmos. Sci.* **56**, 127–150 (1999).
20. E. Boesche, P. Stammes, T. Ruhtz, R. Preusker, and J. Fischer, "Effect of aerosol microphysical properties on polarization of skylight: sensitivity study and measurements," *Appl. Opt.* **45**, 8790–8805 (2006).
21. W. H. Knap, L. C. Labonnote, G. Brogniez, and P. Stammes, "Modeling total and polarized reflectances of ice clouds: evaluation by means of POLDER and ATSR-2 measurements," *Appl. Opt.* **44**, 4060–4073 (2005).
22. K. L. Coulson, *Polarization and Intensity of Light in the Atmosphere* (Deepak, 1988).
23. K. Sassen, M. K. Griffin, and G. C. Dodd, "Optical scattering and microphysical properties of subvisible cirrus clouds, and climatic implications," *J. Appl. Meteor.* **28**, 91–98 (1989).
24. M. I. Mishchenko, I. V. Geogdzhayev, L. Liu, J. A. Ogren, A. A. Lacis, W. B. Rossow, J. W. Hovenier, H. Volten, and O. Muñoz, "Aerosol retrievals from AVHRR radiances: effects of particle nonsphericity and absorption and an updated long-term global climatology of aerosol properties," *J. Quant. Spectrosc. Radiat. Transfer* **79–80**, 953–972 (2003).
25. M. Rast and J. L. Bezy, "ESA medium resolution imaging spectrometer MERIS a review of the instrument and its mission," *Int. J. Remote Sensing* **20**, 1681–1702 (1999).
26. O. P. Hasekamp and J. Landgraf, "Tropospheric ozone information from satellite-based polarization measurements," *J. Geophys. Res.* **107**, 4326 (2002).
27. O. P. Hasekamp, J. Landgraf, and R. van Oss, "The need of polarization modeling for ozone profile retrieval from back-scattered sunlight," *J. Geophys. Res.* **107**, 4692 (2002).
28. D. M. Stam, J. F. De Haan, J. W. Hovenier, and I. Aben, "Detecting radiances in the O₂A band using polarization sensitive satellite instruments, with application to GOME," *J. Geophys. Res.* **105**, 22379–22392 (2000).
29. B. van Diedenhoven, O. P. Hasekamp, and I. Aben, "Surface pressure retrieval from SCIAMACHY measurements in the O₂A band: validation of the measurements and sensitivity on aerosols," *Atmos. Chem. Phys. Discuss.* **5**, 1469–1499 (2005).
30. H. Bovensmann, J. P. Burrows, M. Buchwitz, J. Frerick, S. Noel, V. V. Rozanov, K. V. Chance, and A. P. H. Goede, "SCIAMACHY: mission objectives and measurement modes," *J. Atmos. Sci.* **56**, 127–150 (1999).
31. N. A. J. Schutgens, and P. Stammes, "Parameterization of Earth's polarization spectrum in the ultra-violet," *J. Quant. Spectrosc. Radiat. Transfer* **75**, 239–255 (2002).
32. L. Duforet, R. Frouin, and P. Dubuisson, "Importance and estimation of aerosol vertical structure in satellite ocean-color remote sensing," *Appl. Opt.* **46**, 1107–1119 (2007).
33. J. L. Deuze, P. Goloub, M. Herman, A. Marchand, G. Perry, S. Susana, and D. Tanre, "Estimate of the aerosol properties over the ocean with POLDER on ADEOS-1," *J. Geophys. Res.* **105**, 15329–15346 (2000).
34. M. I. Mishchenko, B. Cairns, G. Kopp, C. F. Schueler, B. A. Fafaul, J. E. Hansen, R. J. Hooker, T. Itchkawich, H. B. Maring, and L. D. Travis, "Precise and accurate monitoring of terrestrial aerosols and total solar irradiance: introducing the Glory Mission," *Bull. Am. Meteorol. Soc.* **88**, 677–691 (2007).
35. D. M. O'Brien and P. J. Rayner, "Global observations of the carbon budget, 2, CO₂ column from differential absorption of reflected sunlight in the 1.61 μm band of CO₂," *J. Geophys. Res.* **107**, 4354 (2002).
36. D. Crisp, R. M. Atlas, F.-M. Breon, L. R. Brown, J. P. Burrows, P. Ciaia, B. J. Connor, S. C. Doney, I. Y. Fung, D. J. Jacob, E. C. Miller, D. O'Brien, S. Pawson, J. T. Randerson, P. Rayner, R. J. Salawitch, S. P. Sander, B. Sen, G. L. Stephens, P. P. Tans, G. C. Toon, P. O. Wennberg, S. C. Wofsy, Y. L. Yung, Z. Kuang, B. Chudasama, G. Sprague, B. Weiss, R. Pollock, D. Kenyon, and S. Schroll, "The Orbiting Carbon Observatory (OCO) mission," *Adv. Space Res.* **34**, 700–709 (2004).
37. R. E. Haring, R. Pollock, B. M. Sutin, and D. Crisp, "Development status of the Orbiting Carbon Observatory instrument optical design," *Proc. SPIE* **5883**, 61–70 (2005).